

This work was written as part of one of the author's official duties as an Employee of the United States Government and is therefore a work of the United States Government. In accordance with 17 U.S.C. 105, no copyright protection is available for such works under U.S. Law.

Public Domain Mark 1.0

<https://creativecommons.org/publicdomain/mark/1.0/>

Access to this work was provided by the University of Maryland, Baltimore County (UMBC) ScholarWorks@UMBC digital repository on the Maryland Shared Open Access (MD-SOAR) platform.

**Please provide feedback**

Please support the ScholarWorks@UMBC repository by emailing [scholarworks-group@umbc.edu](mailto:scholarworks-group@umbc.edu) and telling us what having access to this work means to you and why it's important to you. Thank you.

# Atmospheric sulfur cycle simulated in the global model GOCART: Model description and global properties

Mian Chin,<sup>1,2</sup> Richard B. Rood,<sup>2</sup> Shian-Jiann Lin,<sup>2</sup>  
Jean-Francois Müller,<sup>3</sup> and Anne M. Thompson<sup>2</sup>

**Abstract.** The Georgia Tech/Goddard Global Ozone Chemistry Aerosol Radiation and Transport (GOCART) model is used to simulate the atmospheric sulfur cycle. The model uses the assimilated meteorological data from the Goddard Earth Observing System Data Assimilation System (GEOS DAS). Global sulfur budgets from a 6-year simulation for SO<sub>2</sub>, sulfate, dimethylsulfide (DMS), and methanesulfonic acid (MSA) are presented in this paper. In a normal year without major volcanic perturbations, about 20% of the sulfate precursor emission is from natural sources (biogenic and volcanic), and 80% is anthropogenic; the same sources contribute 33% and 67%, respectively, to the total sulfate burden. A sulfate production efficiency of 0.41–0.42 is estimated in the model, an efficiency which is defined as a ratio of the amount of sulfate produced to the total amount of SO<sub>2</sub> emitted and produced in the atmosphere. This value indicates that less than half of the SO<sub>2</sub> entering the atmosphere contributes to the sulfate production, the rest being removed by dry and wet depositions. In a simulation for 1990 we estimate a total sulfate production of 39 Tg S yr<sup>−1</sup>, with 36% and 64% from in-air and in-cloud oxidation, respectively, of SO<sub>2</sub>. We also demonstrate that major volcanic eruptions, such as the Mount Pinatubo eruption in 1991, can significantly change the sulfate formation pathways, distributions, abundance, and lifetime. Comparison with other models shows that the parameterizations for wet removal or wet production of sulfate are the most critical factors in determining the burdens of SO<sub>2</sub> and sulfate. Therefore a priority for future research should be to reduce the large uncertainties associated with the wet physical and chemical processes.

## 1. Introduction

The important roles of sulfate aerosol in global climate change, atmospheric chemistry, and environmental health have been well recognized in recent years. Sulfate aerosol is one of the major aerosol types in the troposphere with a dominant anthropogenic component. It affects the Earth's radiative balance directly by scattering solar radiation and indirectly by forming new clouds and modifying cloud properties. It also provides surfaces for heterogeneous reactions to take place, thus altering the concentrations of many important atmospheric species. Sulfate can also interact with

other types of aerosols, such as dust and carbonaceous aerosols, to modify their hygroscopic properties when internally mixed with them. The fundamental step toward quantifying all the direct and indirect effects of sulfate aerosol is determining its spatial and temporal distributions and the various processes that control the distributions.

There have been numerous observational data of aerosols and their precursors obtained at ground sites, in field campaigns, and from satellite measurements. However, measurements at the surface or in field campaigns are limited in spatial or temporal coverage, while satellite observations are limited in measurable quantities. Therefore a global model is needed to integrate the spaceborne, airborne, and ground-based data in order to interpret the data in a broader context. In fact, several global models have been used to study the tropospheric sulfur cycle since 1991 [e.g., *Langner and Rodhe*, 1991; *Pham et al.*, 1995; *Feichter et al.*, 1996; *Chin et al.*, 1996; *Chuang et al.*, 1997; *Roelofs et al.*, 1998; *Koch et al.*, 1999; *Barth et al.*, 2000; *Rasch et al.*, 2000]. Almost all the published global sulfur models were either driven by the off-line meteorological fields generated in general circulation models (GCM), or were coupled

<sup>1</sup>School of Earth and Atmospheric Sciences, Georgia Institute of Technology, Atlanta.

<sup>2</sup>NASA Goddard Space Flight Center, Greenbelt, Maryland.

<sup>3</sup>Belgian Institute for Space Aeronomy, Brussels, Belgium.

on-line with the GCM. Although these model studies have helped to advance our understanding of the tropospheric sulfur cycle, it is often difficult for them to explain the observed day-to-day and year-to-year variability, let alone to interpret in situ data from fields campaigns. This is mainly because the results from the GCM models in general represent multiyear values averaged over a large area, which is inappropriate for comparisons with observations in a specific time.

Here we introduce the Georgia Tech/Goddard Global Ozone Chemistry Aerosol Radiation and Transport (GOCART) model, which can be potentially the most suitable tool to link the satellite and in situ observations. The main advantage of the model, which is also the main difference between this model and the previously published models, is that the GOCART model is driven by the assimilated meteorological fields, which are generated in the Goddard Earth Observing System Data Assimilation System (GEOS DAS). This type of model is therefore appropriate for interpreting measurements for a specific period of time. In addition, because the GOCART model is a global-scale model, it is also convenient to use in analyzing satellite data and conducting global assessments.

In this paper, we provide a detailed description of the model components used for simulating the tropospheric sulfur cycle (section 2). The global distributions and 6-year budgets for sulfate and its precursors are presented (section 3), and the anthropogenic contribution to the sulfate burden is discussed (section 5). Results from our model are compared with those from most recent model studies [Koch *et al.*, 1999; Barth *et al.*, 2000; Rasch *et al.*, 2000] (sections 4 and 5). A detailed evaluation of the model results with observations and budgets for several continental and oceanic regions are presented in a companion paper [Chin *et al.*, this issue]. It is noted that in addition to sulfate, other aerosol components are also simulated in the GOCART model, which include dust (P. Ginoux *et al.*, manuscript in preparation, 2000), carbonaceous, and sea-salt aerosols (in progress). With all the major aerosols simulated, we will be able to compare the aerosol properties generated in the model with those retrieved from the satellite measurements, and apply the model to global aerosol analysis.

## 2. Model Description

### 2.1. Model Framework

The GOCART model uses the GEOS DAS assimilated meteorological data [Schubert *et al.*, 1993]. The spatial resolution of the model is the same as in the GEOS DAS, which has a horizontal resolution of 2° latitude by 2.5° longitude. The vertical resolution varies with different versions of the GEOS DAS. There are 20 vertical sigma levels in version 1 (GEOS 1, available for the period of January 1980 to November 1995), extending from the surface to 10 mbar [Allen *et al.*, 1996; Chin *et al.*, 1998]. In version GEOS 1.3 (available

**Table 1.** GEOS DAS Meteorological Fields Used in the GOCART Model

| GEOS DAS Fields                              | Time, hours | Quantity <sup>a</sup> |
|--|-------------|-----------------------|
| Surface pressure                             | 6           | I                     |
| Temperature                                  | 6           | I                     |
| Wind velocity                                | 6           | I                     |
| Specific humidity                            | 6           | I                     |
| Surface albedo                               | 6           | I                     |
| Surface type (land, water, or ice)           | 6           | I                     |
| Cloud mass flux                              | 6           | A                     |
| Convective cloud detrainment                 | 6           | A                     |
| Specific humidity change                     | 6           | A                     |
| Aerodynamic resistance <sup>b</sup>          | 6           | A                     |
| Turbulent diffusion coefficient <sup>b</sup> | 3           | A                     |
| Wind velocity at 10 m <sup>c</sup>           | 3           | A                     |
| Cloud fraction (column)                      | 3           | A                     |
| Boundary layer depth                         | 3           | A                     |
| Surface friction velocity                    | 3           | A                     |
| Surface roughness length                     | 3           | A                     |
| Surface air temperature                      | 3           | A                     |
| Surface net shortwave radiation              | 3           | A                     |
| Surface sensible heat flux                   | 3           | A                     |
| Surface precipitation, total                 | 3           | A                     |
| Surface precipitation, convective            | 3           | A                     |

<sup>a</sup>I is instantaneous quantity, A is time averaged quantity.

<sup>b</sup>Aerodynamic resistance and turbulent diffusion coefficients were not archived in the earlier version of GEOS DAS (before 1997). They have been calculated using the archived GEOS DAS fields for simulations before 1997.

<sup>c</sup>The 10 m winds over the oceans are replaced by the 6-hour instantaneous remote sensing data from the SSM/I. See text for details.

from April 1995 to November 1997), designed to support the Stratospheric Tracers of Atmospheric Transport (STRAT) mission, there are 46 vertical levels with approximately 26 of them in the stratosphere and the model top at 0.1 mbar. In our tropospheric simulation we have aggregated the top 23 levels (from 40 mbar to 0.1 mbar) in the GEOS 1.3 to 3 levels and kept the lowest 23 levels (from surface to 40 mbar) as the same resolution as in the GEOS 1.3 such that the total number of model vertical levels is 26. The lowest five layers in both GEOS 1 and GEOS 1.3 are centered at approximately 50, 250, 600, 1100, and 1800 m above the surface. Newer versions of the GEOS DAS data, for example, GEOS 2 and GEOS 3, with higher vertical or horizontal resolutions have become available for the time periods after November 1997.

The GEOS DAS meteorological data contain not only prognostic fields, such as horizontal winds, temperature, and pressure, but also extensive diagnostic fields, such as cloud mass flux, surface precipitation rates, boundary layer height, and surface roughness. Table 1 lists the GEOS DAS archived prognostic and diagnostic fields used in our sulfur simulations.

We present in this paper a 6-year simulation from 1989 to 1994. Four sulfur species are simulated in

the model: dimethylsulfide (DMS),  $\text{SO}_2$ , sulfate, and methanesulfonic acid (MSA). There are seven modules representing atmospheric processes of these sulfur species: emission, chemistry, advection, convection, diffusion, dry deposition, and wet deposition. The model solves the continuity equation using the method of operator splitting. The model time step is 20 min for advection, convection, and diffusion, and 60 min for the other processes. The instantaneous meteorological fields in Table 1 are linearly interpolated to the model time. Initialization was done for the last 3 months of 1988, starting from low concentrations (0.1 ppt) for all four sulfur species.

## 2.2. Transport

The advection and convection schemes used in the model have been described in detail elsewhere [Allen *et al.*, 1996]. Here, briefly, advection is computed by a flux-form semi-Lagrangian method [Lin and Rood, 1996]. Moist convection is parameterized using archived cloud mass flux fields from the GEOS DAS. In the previous model studies using the GEOS DAS fields, the boundary layer mixing was parameterized such that a fixed fraction of material was uniformly mixed within the boundary layer [Allen *et al.*, 1996; Chin *et al.*, 1998]. It was found very difficult to choose a universal value of the mixing fraction since it does not reflect the boundary layer turbulence [Chin *et al.*, 1998]. In the GOCART model the boundary layer turbulent mixing is computed using a second-order closure scheme [Helfand and Labraga, 1988], which was also used in the GEOS DAS analysis for heat and moisture turbulent mixing [Takacs *et al.*, 1994]. The scheme takes into account both growing and decaying turbulence. The turbulent diffusion coefficient is a function of the turbulent kinetic energy, the buoyancy, and wind shear parameters.

## 2.3. Sulfur Emissions

The GOCART model includes emissions of DMS from the ocean,  $\text{SO}_2$  and sulfate from anthropogenic activities, and  $\text{SO}_2$  from biomass burning, aircraft exhaust, and volcanic eruptions. Figure 1 shows an annually averaged emission flux from anthropogenic and natural sources (DMS and volcanic  $\text{SO}_2$ ) for 1990.

Anthropogenic emissions are taken from the Emission Database for Global Atmospheric Research (EDGAR) for the year of 1990 [Olivier *et al.*, 1996]. The annual total emission rate is  $72.8 \text{ Tg S yr}^{-1}$  which includes emissions from industrial processes ( $59.3 \text{ Tg S yr}^{-1}$ ), residential and commercial consumptions ( $8.5 \text{ Tg S yr}^{-1}$ ), and transportation (road, rail, and shipping,  $5.0 \text{ Tg S yr}^{-1}$ ). The fraction of direct sulfate emission has been estimated from 1.4% to 5% of the total emission [Benkovitz *et al.*, 1996]; we assume here a fraction of 5% for Europe and 3% for elsewhere. The rest is emitted as  $\text{SO}_2$ . Emission rates are assumed to be constant throughout the year except for Europe, where a seasonal variation is imposed such that the emission rates are maximum in winter (30% higher than the annual average) and minimum in summer (30% lower than the annual average). This seasonal variation reflects mainly the demand for domestic heating [Sandnes and Styve, 1992].

Emission of DMS from the ocean is calculated as a product of the seawater DMS concentration and sea-to-air transfer velocity. Monthly averaged surface seawater DMS concentrations in  $1^\circ \times 1^\circ$  grid resolution are taken from Kettle *et al.* [1999]. This seawater DMS concentration map is generated based on the compilation of a database of over 15,000 measurements around the globe. The transfer velocity of DMS is computed using an empirical formula from Liss and Merlivat [1986],

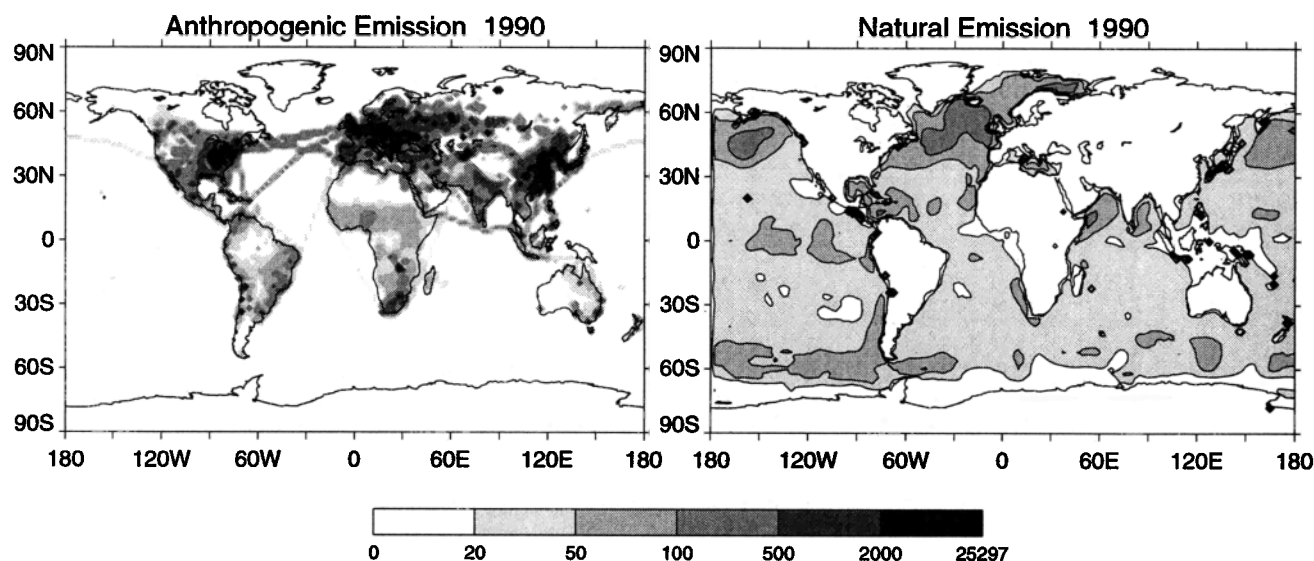


**Figure 1.** Annual emissions ( $\text{mg S m}^{-2} \text{ yr}^{-1}$ ) of sulfate precursors in 1990 from anthropogenic and natural (oceanic and volcanic) sources used in the model.

which assumes linear relationships between the transfer velocity and the 10-m wind speed. Diffusion of DMS within the ocean surface water is taken into account as a function of sea surface temperature [Saltzman *et al.*, 1993]. The 10-m winds used in the model are the remote sensing data from the Special Sensor Microwave Imager (SSM/I) operated on a series of satellites in the Defense Meteorological Satellite Program [Atlas *et al.*, 1996]. The SSM/I winds have been found to represent accurately the local observations [Chin *et al.*, 1998]. It has been noted that there could be a factor of 2 or more differences in the transfer velocity calculated from different formulae [e.g., Smethie *et al.*, 1985; Wanninkhof, 1992; Erickson, 1993], and a single parameterization of transfer velocity based on wind speed alone is not sufficient to describe DMS flux from the different regions of the oceans [Chin *et al.*, 1998].

Volcanic sources of SO<sub>2</sub> include emissions from both continuously active and sporadically erupting volcanoes. The continuous volcanic emissions are taken from a database of Andres and Kasgnoc [1998]. The database includes SO<sub>2</sub> released from 49 volcanoes which have been continuously active over the last 25 years with an emission rate of 4.8 Tg S yr<sup>-1</sup>. We assume that SO<sub>2</sub> is injected at a constant rate within 1 km above the crater altitudes. For the sporadically erupting volcanoes we use the volcanic database from the Smithsonian Global Volcanism Program [Simkin and Siebert, 1994] which has documented the locations, the erupting dates and duration, and the volcanic explosivity index (VEI) up to 1994. We then use the VEI to estimate the volcanic cloud height [Simkin and Siebert, 1994], and obtain the amount of SO<sub>2</sub> emitted to the atmosphere by a relationship between the VEI and SO<sub>2</sub> flux [Schnetzler *et al.*, 1997]. When they become available, satellite-observed volcanic SO<sub>2</sub> emission data from the Total Ozone Monitoring Spectroscopy (TOMS) instrument [Bluth *et al.*, 1997] are used to replace the calculated emission rates. We further assume that SO<sub>2</sub> is injected within a slab which is located at the top portion of the erupting volcanic cloud with a thickness of 1/3 of the cloud column (L. Glaze, personal communication, 1998). This assumption is based on the observations of plume height and thickness after eruption [e.g., McCormick *et al.*, 1995] and the results from volcanic plume dispersion models [e.g., Suzuki, 1983].

Other sources of SO<sub>2</sub> in the model include biomass burning (2.3 Tg S yr<sup>-1</sup>) and aircraft emissions (0.07 Tg S yr<sup>-1</sup>). Seasonal biomass burning emissions are from Spiro *et al.* [1992]. Aircraft emission is calculated based on the monthly averaged fuel consumption inventory for 1992 from NASA's Atmospheric Effects of Aviation Project (AEAP), assuming an emission index of 1.0, that is, 1 g SO<sub>2</sub> emitted per kg fuel burned [Weisenstein *et al.*, 1996].

In our 6-year simulation presented in this paper, we have used the same seasonal emissions from anthropogenic, biomass burning, aircraft, and continuously

active volcanic sources for every year. The only interannually variable sources are the emissions from sporadically erupting volcanoes (based on documented events) and DMS from the ocean (due to the change of surface wind speeds).

## 2.4. Chemistry

Chemical reactions included in the model as follows: DMS oxidation by OH during the day to form SO<sub>2</sub> and MSA, and by nitrate radicals (NO<sub>3</sub>) at night to form SO<sub>2</sub>; SO<sub>2</sub> oxidation by OH in air and by H<sub>2</sub>O<sub>2</sub> in cloud to form sulfate. Reaction rates are taken from DeMore *et al.* [1997]. The yields of SO<sub>2</sub> and MSA from DMS+OH reaction are assumed to be the same as in the work of Chin *et al.* [1996], that is, 100% SO<sub>2</sub> from the abstraction channel, and 75% SO<sub>2</sub> and 25% MSA from the addition channel. We prescribe concentrations of OH, NO<sub>3</sub>, and H<sub>2</sub>O<sub>2</sub> from the monthly averaged fields generated in the Intermediate Model of Global Evolution of Species (IMAGES) [Müller and Brasseur, 1995]. Figure 2 plots the zonally averaged concentrations of OH and H<sub>2</sub>O<sub>2</sub> for January and July. A diurnal variation of OH concentrations is imposed by scaling the average OH fields to the cosine of solar zenith angle. Since the concentrations of NO<sub>3</sub> over the ocean at night are always orders of magnitude higher than those during the day, they are assumed to be zero in the daytime and are evenly distributed over the night.

Because cloud water content is not available in GEOS 1 and GEOS 1.3, we parameterize the in-cloud oxidation of SO<sub>2</sub> by H<sub>2</sub>O<sub>2</sub> as a function of cloud fraction, following Chin *et al.* [1996]. Cloud fraction  $f_c$  for each grid box is assumed as an empirical function of the relative humidity in that grid box, following Sundqvist *et al.* [1989]:

$$f_c = 1 - \sqrt{1 - \frac{r - r_0}{1 - r_0}}$$

where  $r$  is the relative humidity and  $r_0$  is the threshold relative humidity for condensation specified as a function of pressure [Xu and Krueger, 1991]. Within the cloud fraction we assume that the formation of sulfate is determined by the concentration of the limiting reagent, that is, the lesser amount between SO<sub>2</sub> and H<sub>2</sub>O<sub>2</sub>. During the chemistry time step (1 hour), H<sub>2</sub>O<sub>2</sub> is depleted as the aqueous phase reaction of SO<sub>2</sub>+H<sub>2</sub>O<sub>2</sub> can be completed in less than 1 hour [Daum *et al.*, 1984]. The recovery time of H<sub>2</sub>O<sub>2</sub> varies considerably in the literature, from instantaneous replenishment to a day in winter [Koch *et al.*, 1999]. Here we assume that H<sub>2</sub>O<sub>2</sub> is regenerated to its prescribed value every 3 hours, similar to the timescale used by Chin *et al.* [1996].

## 2.5. Dry Deposition

Dry deposition velocities for SO<sub>2</sub>, sulfate, and MSA are calculated in the model using the resistance-in-series scheme [Wesely and Hicks, 1977]. In this scheme, dry deposition velocities are determined as a reciprocal of

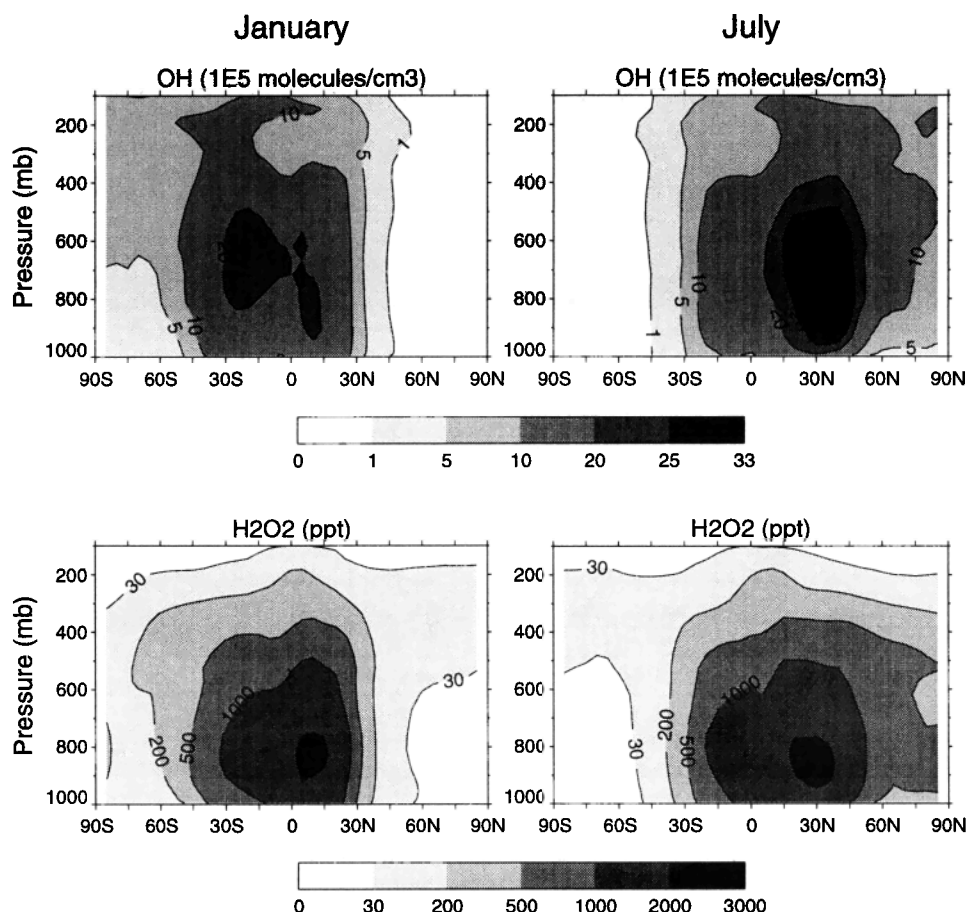


**Figure 2.** Zonal distributions of OH and H<sub>2</sub>O<sub>2</sub> for January and July from the IMAGES model [Müller and Brasseur, 1995].

the sum of aerodynamic resistance, sublayer resistance, and surface resistance. The aerodynamic resistance is taken from the GEOS DAS archive, which is a product of the exchange coefficient for heat and moisture and the surface friction velocity. The sublayer and surface resistance for SO<sub>2</sub> and sulfate are calculated using the formulation of Walcek *et al.* [1986] and Wesely [1989]. The dry deposition velocity of MSA is assumed to be the same as that of sulfate. We impose a minimum SO<sub>2</sub> dry deposition velocity of 0.2 cm s<sup>-1</sup> over the ice and snow and in the polar regions [Voldner *et al.*, 1986; Tarrason and Iversen, 1998]. Typically, the diurnally averaged dry deposition velocity for SO<sub>2</sub> over the land is 0.2–0.4 cm s<sup>-1</sup>, but it varies significantly over the ocean from 0.6 to 0.8 cm s<sup>-1</sup> under stable conditions to 1 to 2 cm s<sup>-1</sup> under unstable conditions. For sulfate a value of 0.08–0.12 cm s<sup>-1</sup> is found over the oceans, and 0.1–0.3 is found over the land except at latitudes higher than 60° in the winter season (0.01–0.05 cm s<sup>-1</sup>). These values are in general consistent with the data from limited direct measurements and with other calculated values [e.g., Voldner *et al.*, 1986; Walcek *et al.*, 1986; Ganzeveld *et al.*, 1998, and references therein].

## 2.6. Wet Scavenging

Wet scavenging of soluble species in the model includes rainout (in-cloud precipitation) and washout (below cloud precipitation) in large-scale precipitation and in deep convective cloud updraft. The GEOS DAS diagnoses the total precipitation at the ground as a column integral of specific humidity change due to moist processes [Takacs *et al.*, 1994]. Here we normalize the precipitation rates from the GEOS DAS to those from an observation-based data product, which is a merged data set combining satellite observations, ground station rain gauge measurements, and the GEOS DAS precipitation fields [Huffman *et al.*, 1997; P. Houser, manuscript in preparation, 2000]. Distribution of large-scale precipitation in a vertical column is estimated based on the specific humidity changes diagnosed in the GEOS DAS:

$$P_{ls}(k) = c \Delta q_t(k) \frac{Q_{ls}}{Q_t}$$

where  $P_{ls}(k)$  is the large-scale precipitation rate at level  $k$ ,  $Q_{ls}$  and  $Q_t$  are the column integrated specific humidity change due to large-scale or total (large-scale and

convective) moist process, respectively,  $c$  is the ratio of the precipitation rate in the merged product to that in the GEOS DAS, and  $\Delta q_t(k)$  is the total specific humidity change at level  $k$  where a negative value indicates a precipitation and a positive value implies an evaporation.

Removal of sulfate and MSA by large-scale rain is calculated as a first-order loss process using parameters of *Giorgi and Chameides* [1986]. The change of aerosol mixing ratio within a model time step is

$$\Delta\chi(k) = \chi(k)f(k)(e^{-\beta(k)\Delta t} - 1)$$

where  $\chi(k)$  is the mixing ratio at level  $k$ ,  $f(k)$  is the fraction of the grid box experiencing precipitation,  $\beta(k)$  is the frequency of cloud to rain conversion, and  $\Delta t$  is the duration of precipitation, which is equal to the wet scavenging time step for large-scale rain. The values of  $f(k)$  and  $\beta(k)$  are defined by the precipitation amount at each grid box and by a typical liquid water content for large-scale precipitation [*Giorgi and Chameides*, 1986].

Washout between the cloud layers or below the lowest cloud level is also computed as a first-order loss process, similar to the treatment of rainout. In this case, the fraction of a grid box with precipitation is determined by the largest value of  $f$  from the overhead rainy grid box, and  $\beta$  is assumed to be  $0.1 \text{ mm}^{-1}$  normalized to the precipitation rate [*Dana and Hales*, 1976]. A fraction of soluble species between or below clouds releases into the grid box if evaporation ( $\Delta q_t > 0$ ) occurs. This fraction is assumed to be the same as that of evaporated water.

It has been found in previous model investigations as well as in field studies that soluble species are scavenged efficiently within the convective cloud updraft [*Balkanski et al.*, 1993; *Cohan et al.*, 1999]. Adapting the principle of *Balkanski et al.* [1993], we couple the convective scavenging with the moist convection process in our model, and use a scavenging efficiency of  $0.4 \text{ km}^{-1}$  for soluble aerosol species.

We use the same method for  $\text{SO}_2$  wet scavenging as that described by *Chin et al.* [1996]: we define a soluble fraction of  $\text{SO}_2$  as limited by the availability of  $\text{H}_2\text{O}_2$  in the precipitating grid box, and scavenge the soluble  $\text{SO}_2$  at the same rate as sulfate. When evaporation occurs, a fraction of dissolved  $\text{SO}_2$  returns to the grid box as sulfate.

### 3. Global Budget and Distributions

#### 3.1. Summary of Global Budget

Summary of a 6-year budget of 1989–1994 is presented in Figure 3. Before we discuss the budget, we shall clarify the terms used in our wet removal and aqueous-phase oxidation budgets since they can sometimes cause confusion. Here the term “wet scavenging” refers to the loss of a particular tracer in the wet process described in section 2.6 regardless of its transformation within the rainwater. With that in mind, we count the

amount of  $\text{SO}_2$  scavenged and subsequently converted to sulfate in the rainwater as a term of wet scavenging of  $\text{SO}_2$ , not sulfate. Also, we do not record this amount as a part of “in-cloud sulfate production” (except for the fraction returned to the atmosphere during the evaporation of raindrops) because the production of sulfate from the dissolved  $\text{SO}_2$  in rainwater does not contribute to either the sulfate burden in the atmosphere or the removal of sulfate from the atmosphere. While it seems just a labeling issue for the sulfur budget, counting the wet scavenging of  $\text{SO}_2$  as a loss of sulfate can lead to an underestimation of atmospheric sulfate lifetime since the lifetime is simply the ratio of atmospheric burden to the loss rate.

As shown in Figure 3, the anthropogenic emission is  $75 \text{ Tg S yr}^{-1}$ , which includes emissions from industrial activities, fuel combustion, ship, and aircraft, as well as from biomass burning. Biogenic emission of DMS from the ocean varies from  $13.3$  to  $15.0 \text{ Tg S yr}^{-1}$ , reflecting the changes in the surface wind speeds. Volcanic emissions are also fairly constant from year to year ( $5.4$ – $6.0 \text{ Tg S yr}^{-1}$ ), except 1991 when a major volcanic eruption of Mount Pinatubo occurred in June, injecting about  $10 \text{ Tg S}$  (or  $20 \text{ Mton SO}_2$ ) into the atmosphere. Total volcanic emission for 1991 is  $19.6 \text{ Tg S yr}^{-1}$ . In a normal year (e.g., without major volcanic eruptions) the fraction of sulfur emitted from natural sources (biogenic and volcanic) is about 20% of the total emission of  $94 \text{ Tg S yr}^{-1}$ .

In-cloud oxidation of  $\text{SO}_2$  is responsible for about 64% of total sulfate production in a normal year, while in-air oxidation accounts for the rest 36%. In contrast, less than half of the sulfate production in 1991 takes place in-cloud because the Pinatubo eruption injects most  $\text{SO}_2$  into the stratosphere where the gas-phase reaction with OH is the only mechanism in the model to convert  $\text{SO}_2$  to sulfate. Dry deposition and wet scavenging remove roughly the same amount of sulfur from the atmosphere ( $45$ – $55 \text{ Tg S yr}^{-1}$ ). While dry deposition is the most important loss of  $\text{SO}_2$  (45%) followed by in-cloud oxidation (27%), wet scavenging eliminates 90% of sulfate produced in the atmosphere. The lifetime is 1.8 days for  $\text{SO}_2$  and 5.8 days for sulfate in a normal year.

The annually averaged atmospheric burden for  $\text{SO}_2$  is  $0.42$ – $0.48 \text{ Tg S}$  except 1991. The  $\text{SO}_2$  burden is  $1.6 \text{ Tg S}$  in 1991, with most of it residing in the stratosphere, that is, above  $100$ – $120 \text{ mbar}$  in the model (Figure 3). While  $\text{SO}_2$  returns to its normal level rather quickly after the Pinatubo eruption ( $e$ -folding time about 1 month), it takes much longer for sulfate to relax back to its normal level. As illustrated in Figure 3, 3 years after the Pinatubo eruption, total sulfate burden in 1994 ( $0.98 \text{ Tg S}$ ) is still significantly higher than its pre-Pinatubo value in 1989–1990 ( $0.63 \text{ Tg S}$ ).

The only removal process for DMS is its oxidation in the atmosphere. Globally, nearly 90% of DMS emitted from the ocean is oxidized by OH during the day; only

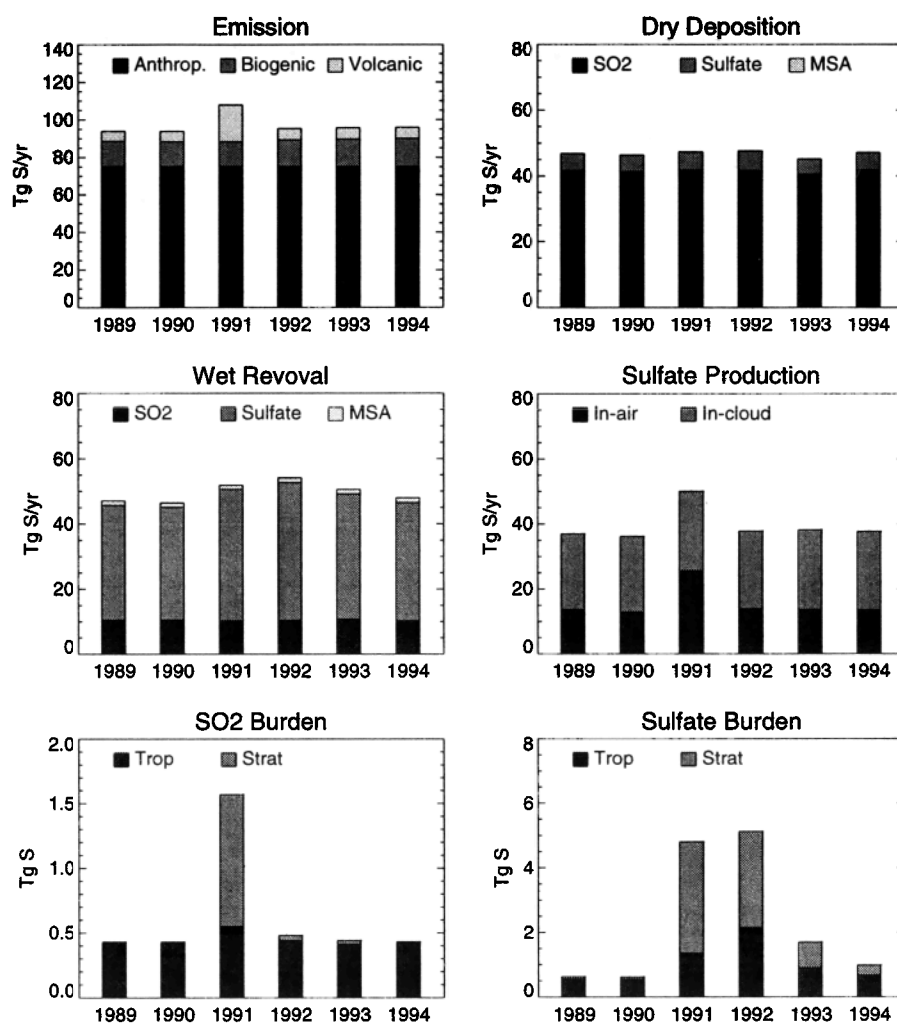


**Figure 3.** Summary of a 6-year sulfur budget (1989-1994) in the GOCART model. Troposphere and stratosphere interface at 120-100 mbar.

10% is lost at night via reaction with  $\text{NO}_3$ . The stable products from DMS oxidation are 89%  $\text{SO}_2$ , which can be further oxidized to sulfate, and 11% MSA, which is removed by wet (91%) and dry (9%) depositions. The atmospheric burden for DMS is 0.072–0.080 Tg S, and that for MSA is 0.027–0.032 Tg S. The lifetime is 1.9–2.2 days for DMS and 6.8–7.2 days for MSA.

We define a term of the sulfate production efficiency as the amount of sulfate produced relative to the total amount of  $\text{SO}_2$  emitted and produced in the atmosphere. The sulfate production efficiency is a direct measure of the effectiveness of  $\text{SO}_2$  oxidation versus the dry and wet removal of  $\text{SO}_2$ . We find in our model a typical production efficiency value of 0.41–0.42, which indicates that only less than half of the  $\text{SO}_2$  contributes to sulfate production in the atmosphere, and the rest is mainly deposited to the surface. In the Pinatubo eruption year of 1991, however, the sulfate production efficiency increases to 0.49, reflecting that the  $\text{SO}_2$  released at high altitudes produces sulfate much more effectively than that emitted near the surface.

### 3.2. Global Distributions

To present some general features simulated in the model, we plot in Figure 4 global distributions of  $\text{SO}_2$ , sulfate, DMS, and MSA at the surface (Figure 4a) and at 500 mbar (Figure 4b) for the pre-Pinatubo year of 1990. Concentrations shown in Figure 4 are average values for two seasons: December, January, February (DJF), and June, July, August (JJA). High surface concentrations of  $\text{SO}_2$  and sulfate are found in regions of high anthropogenic emissions for both seasons, as expected. The major contrast between DJF and JJA is the strong advection of pollutants from the midlatitude source regions to the Arctic circle in DJF. While  $\text{SO}_2$  concentrations are higher in the winter than in the summer, the reverse is true for sulfate because of the seasonal variation of  $\text{SO}_2$  oxidation rates. Globally, the sulfate production efficiency in January is only 0.27, whereas in July it is 0.48 in 1990.

The distribution of DMS at the surface closely resembles that in seawater. Very high surface air concentra-



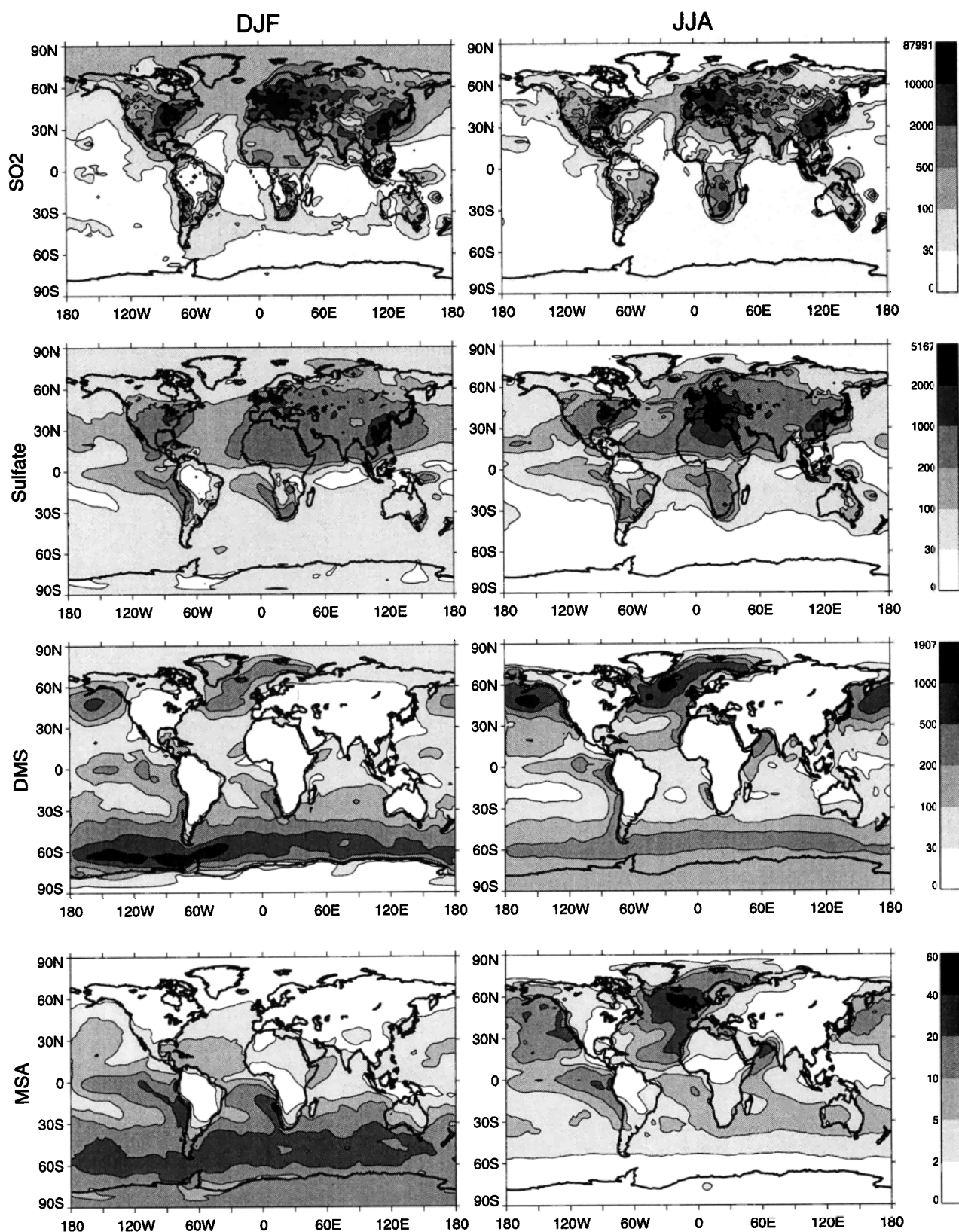


**Figure 4a.** Distributions of sulfur species (ppt) in DJF and JJA at the surface in the simulation for 1990.

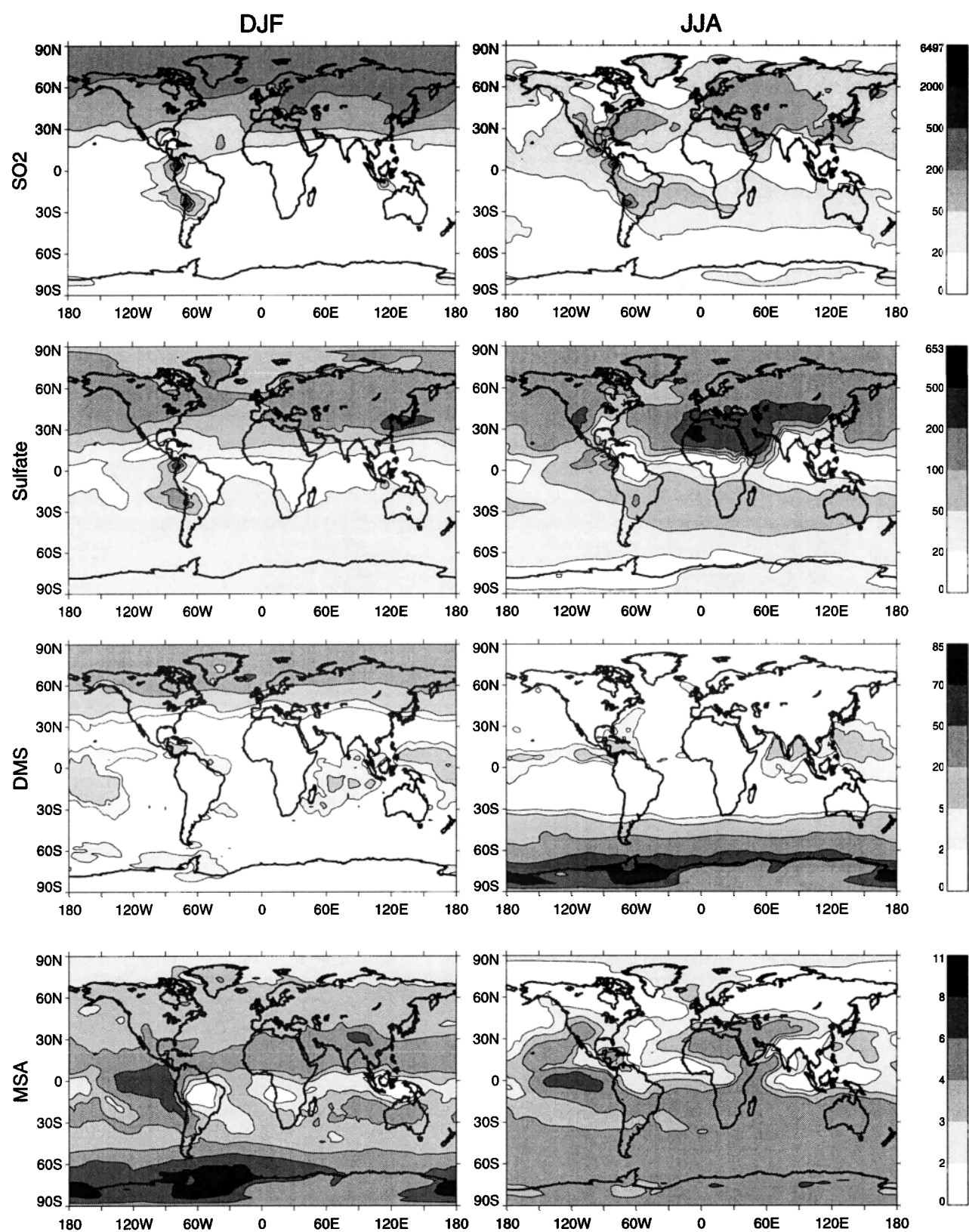


**Figure 4b.** Same as Figure 4a, but at 500 mbar.

tions of DMS (500–2000 ppt) are produced in the model near 60° latitude in the summer hemisphere. These elevated concentrations are directly related to the high DMS emission flux ( $10\text{--}50\ \mu\text{mol m}^{-2}\text{ d}^{-1}$ ), a product of very high seawater DMS concentrations and strong surface winds. While the surface DMS concentrations at these latitudes in summer seem too high compared with some measurements near the Antarctic coast ( $< 800\text{ ppt}$  [Staubes and Georgii, 1993; Berresheim et al., 1998]), the model-calculated concentrations of the DMS oxidation products, sulfate and MSA, at high-latitude sites (e.g., Palmer Station and Mawson in Antarctica, and Haemey in Iceland) agree with the observations to within 40% [Chin et al., this issue]. This apparent inconsistency needs to be further investigated. Finally, as expected, MSA surface distribution is similar to that of DMS.

One common feature for all sulfur species at 500 mbar (Figure 4b) is that they are better mixed zonally and the concentrations are 1 to 2 magnitudes lower than that at the surface, reflecting their relatively short lifetimes (several days). DMS concentrations at 500 mbar are higher in the winter hemisphere than in the summer hemisphere, opposite to the pattern found at the surface. This is because the slow oxidation rates of DMS in winter allow DMS to be transported to higher altitudes. On the other hand, the DMS loss rates are

higher in summer than in winter due to the higher OH concentrations; thus only a small fraction of DMS escapes from the boundary layer in summer despite the higher emission rates.

The annually averaged zonal mean distributions of  $\text{SO}_2$ , sulfate, DMS, and MSA for 1990 are shown in Figure 5. As expected, both  $\text{SO}_2$  and sulfate exhibit high concentrations in the northern hemisphere. In the tropics, DMS is pumped to the upper troposphere by the deep convective process. Interestingly, the same process is also responsible for the low sulfate concentration in the middle to upper troposphere over the tropics, thanks to the efficient wet scavenging of sulfate in cloud convection. This feature also appeared in the model simulations of Feichter et al. [1996] and Koch et al. [1999], but was lacking in some other models [e.g., Chin et al., 1996; Barth et al., 2000], depending on the convective process in the meteorological data and the efficiency of in-cloud scavenging in different models.

We plot in Figure 6 the column total sulfate sources and sinks in the 1990 simulation as a function of latitude. It can be seen that in-cloud oxidation of  $\text{SO}_2$  is the most important source of sulfate, especially at high latitudes (60°N and higher in the northern hemisphere, and between 40°S and 70°S in the southern hemisphere), where in-cloud oxidation contributes 80–90% of the total sulfate source. While scavenging by

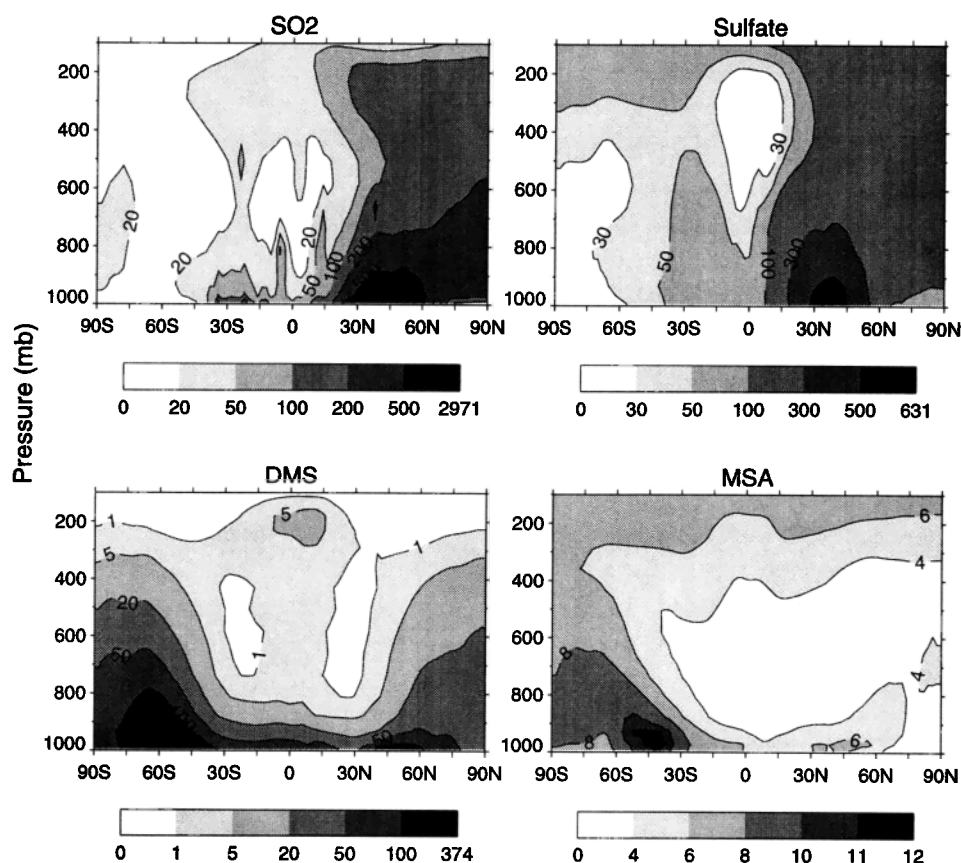


**Figure 5.** Zonal distributions of sulfur species (ppt) in the simulation for 1990.

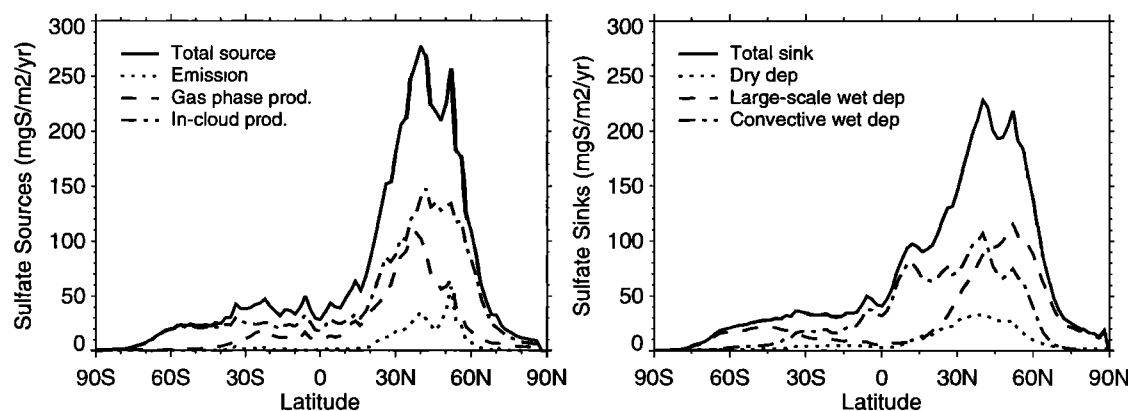


Figure 6. Sources and sinks for sulfate in the 1990 simulation as a function of latitude.

large-scale rain dominates the sulfate loss over mid and high latitudes, wet convective scavenging dominates over the tropics and subtropics. Dry deposition in general accounts for less than 20% of sulfate loss at all latitudes except in the polar regions.

#### 4. Comparisons With Other Global Model Studies

We focus here on the comparison of sulfur budget in the GOCART model simulation for 1990 with two of the most recent global model studies: *Koch et al.* [1999], using the Goddard Institute for Space Studies' general circulation model version II' (GISS GCM), and *Barth et al.* [2000] and *Rasch et al.* [2000], using the National Center for Atmospheric Research Community Climate Model (NCAR CCM3). Intercomparisons involving other earlier models [e.g., *Langner and Rodhe*, 1991; *Pham et al.*, 1995; *Fechter et al.*, 1996; *Chin et al.*, 1996] have been presented in previous model studies [*Chin et al.*, 1996; *Koch et al.*, 1999; *Rasch et al.*, 2000] and will not be discussed in detail here. We will only summarize the major differences between this study and an earlier work [*Chin et al.*, 1996].

Table 2 summarizes the comparison of sulfur budgets among the GOCART, GISS, and NCAR models. Our total emission ( $93.9 \text{ Tg S yr}^{-1}$ ) is higher than that in both GISS and NCAR models ( $83 \text{ Tg S yr}^{-1}$ ). This is because we use the EDGAR database of 1990 emission inventory ( $72.8 \text{ Tg S yr}^{-1}$ ) which also includes emissions from shipping and land use, while the GISS and NCAR models use the 1985 emission inventory ( $67 \text{ Tg S yr}^{-1}$ ) from the Global Emissions Inventory Activity [*Benkovitz et al.*, 1996]. The biomass burning emission in our model is the same as that in the GISS model ( $2.3 \text{ Tg S yr}^{-1}$ ), but the volcanic emission ( $5.5 \text{ Tg S yr}^{-1}$ ) is much higher than that in the GISS model ( $3.5 \text{ Tg S yr}^{-1}$ ) because we include emissions from both continuously active and sporadically erupting volcanoes, while *Koch et al.* [1999] considers only noneruptive volcanoes. Volcanic and biomass burning emissions are not

included in the NCAR model. Emission of DMS calculated in our model is  $13.3 \text{ Tg S yr}^{-1}$  for 1990, about 30% higher than that in the GISS model ( $10.7 \text{ Tg S yr}^{-1}$ ), even though both models use the same formula for transfer velocity and the same DMS seawater concentrations in calculating DMS emission rates. This difference may be attributed to the lower 10-m wind speeds in the GISS GCM. The NCAR model calculates a total DMS emission of  $15.5 \text{ Tg S yr}^{-1}$ , based on the latitudinal bands of DMS flux in the work of *Bates et al.* [1992] and the distribution of the ocean color in the remote sensing products.

Our model estimates an equal amount of sulfur being removed by dry deposition and wet scavenging (50% for each process), while a slightly higher fraction of dry deposition (54% dry, 46% wet) is obtained in the GISS model, and the wet removal is about twice as effective as dry deposition in the NCAR model.

Total sulfate production from  $\text{SO}_2$  oxidation is  $38.5 \text{ Tg S yr}^{-1}$  in our model. Although this value is the lowest among the three models, remember that we do not count the  $\text{SO}_2$  loss in wet scavenging as a part of sulfate production while both the GISS and NCAR models do. As we stated in the previous section, even though the amount of  $\text{SO}_2$  scavenged by the rain is subsequently converted to sulfate in rainwater, this process does not play a role in determining the atmospheric sulfate concentration or removal; we thus consider the in-rain sulfate production as ineffective. Should we include the  $\text{SO}_2$  wet scavenging as a part of sulfate production, the value would be  $49.1 \text{ Tg S yr}^{-1}$  which is between the GISS and NCAR model.

As we have shown in the previous section, 89% of the DMS emitted from the ocean produces  $\text{SO}_2$  ( $11.9 \text{ Tg S yr}^{-1}$ ). Of this amount, 87% is produced via  $\text{DMS} + \text{OH}$ , and 13% is produced via  $\text{DMS} + \text{NO}_3$ . The  $\text{SO}_2$  production is more efficient in the GISS model (93%), whereas the NCAR model assumes  $\text{SO}_2$  as the only DMS oxidation product.

The GISS model has the highest  $\text{SO}_2$  and sulfate burden among the three models, which was attributed to

**Table 2.** Comparison of Sulfur Budget From the GOCART Model With the GISS and NCAR Models

| Budget Component                                  | GOCART <sup>a</sup> |         | GISS <sup>b</sup> |         | NCAR <sup>c</sup> |         |
|---|---------------------|---------|-------------------|---------|-------------------|---------|
| Total emission, Tg S yr <sup>-1</sup>             | 93.9                |         | 83.0              |         | 82.5              |         |
| SO <sub>2</sub> anthropogenic                     | 70.6                | (75.2%) | 64.6              | (77.8%) | 65.7              | (79.6%) |
| SO <sub>2</sub> biomass burning                   | 2.3                 | (2.4%)  | 2.3               | (2.8%)  |                   |         |
| SO <sub>2</sub> volcanic                          | 5.5                 | (5.9%)  | 3.5               | (4.2%)  |                   |         |
| Sulfate anthropogenic                             | 2.2                 | (2.3%)  | 1.9               | (2.3%)  |                   |         |
| DMS oceanic                                       | 13.3                | (14.2%) | 10.7              | (12.9%) | 15.5              | (18.8%) |
| Total deposition, Tg S yr <sup>-1</sup>           | 93.0                |         | 83.4              |         | 81.0              |         |
| SO <sub>2</sub> dry deposition <sup>d</sup>       | 41.2                | (44.3%) | 35.5              | (42.6%) | 24.5              | (30.2%) |
| SO <sub>2</sub> wet scavenging                    | 10.6                | (11.4%) | 0.2               | (0.2%)  | 1.6               | (2.0%)  |
| Sulfate dry deposition                            | 5.1                 | (5.5%)  | 9.2               | (11.0%) | 3.7               | (4.6%)  |
| Sulfate wet scavenging <sup>d</sup>               | 34.7                | (37.3%) | 37.4              | (44.8%) | 51.2              | (63.2%) |
| MSA dry deposition                                | 0.1                 | (0.1%)  | 0.2               | (0.2%)  |                   |         |
| MSA wet scavenging                                | 1.3                 | (1.4%)  | 0.9               | (1.1%)  |                   |         |
| SO <sub>2</sub> production, Tg S yr <sup>-1</sup> | 11.9                |         | 10.0              |         | 15.5              |         |
| From DMS+OH                                       | 10.4                | (87.4%) |                   |         |                   |         |
| From DMS+NO <sub>3</sub>                          | 1.5                 | (12.6%) |                   |         |                   |         |
| Sulfate production, Tg S yr <sup>-1</sup>         | 38.5                |         | 44.7              |         | 53.6              |         |
| In-air  | 14.0                | (36.4%) | 13.1              | (29.3%) | 9.2               | (17.2%) |
| In-cloud <sup>d</sup>                             | 24.5                | (63.6%) | 31.6              | (70.7%) | 44.4              | (82.8%) |
| Burden, Tg S                                      |                     |         |                   |         |                   |         |
| SO <sub>2</sub>                                   | 0.43                |         | 0.56              |         | 0.4               |         |
| Sulfate   | 0.63                |         | 0.73              |         | 0.57              |         |
| DMS   | 0.073               |         | 0.056             |         | 0.06              |         |
| MSA   | 0.028               |         | 0.023             |         |                   |         |
| Lifetime, days                                    |                     |         |                   |         |                   |         |
| SO <sub>2</sub>                                   | 1.8                 |         | 2.6               |         | 1.9               |         |
| Sulfate <sup>e</sup>                              | 5.8                 | (4.6)   | 5.7               |         | 4.0               |         |
| DMS   | 2.0                 |         | 1.9               |         | 1.4               |         |
| MSA   | 7.1                 |         | 7.6               |         |                   |         |
| Loss frequency <sup>f</sup> , day <sup>-1</sup>   |                     |         |                   |         |                   |         |
| SO <sub>2</sub> dry deposition                    | 0.26                |         | 0.17              |         | 0.17              |         |
| SO <sub>2</sub> in-air oxidation                  | 0.09                |         | 0.06              |         | 0.06              |         |
| SO <sub>2</sub> wet processes <sup>g</sup>        | 0.22                |         | 0.15              |         | 0.31              |         |
| Sulfate dry deposition                            | 0.02                |         | 0.03              |         | 0.02              |         |
| Sulfate wet scavenging                            | 0.15                | (0.2)   | 0.14              |         | 0.25              |         |

<sup>a</sup>This work, 1990 simulation.<sup>b</sup>Koch *et al.* [1999].<sup>c</sup>Barth *et al.* [2000] and Rasch *et al.* [2000]<sup>d</sup>Wet scavenging of SO<sub>2</sub> in the GISS and NCAR models was counted as a part of sulfate in-cloud production as well as sulfate wet scavenging budgets. See text for details.<sup>e</sup>The numbers in parentheses for the GOCART model are the values that would be if SO<sub>2</sub> wet scavenging were considered as a part of sulfate wet deposition term, as treated by the GISS and NCAR models. See text for explanation.<sup>f</sup>Loss frequency is defined as the loss rate divided by the burden.<sup>g</sup>Including in-cloud oxidation and wet scavenging.

the use of prognostic H<sub>2</sub>O<sub>2</sub> and an insufficient entrainment of H<sub>2</sub>O<sub>2</sub> from the cloud base to oxidize SO<sub>2</sub> in highly polluted regions [Koch *et al.*, 1999]. On the other hand, the NCAR model also uses prognostic H<sub>2</sub>O<sub>2</sub> but shows the lowest SO<sub>2</sub> and sulfate burden. The cause of the discrepancy is likely a combination of the differences in cloud processing, oxidant concentrations, and precip-

itation rates, among others, between the models. The DMS burden and lifetime in our model is 22% and 41% higher than those in the NCAR model, even though both models have used the same prescribed OH and NO<sub>3</sub> fields for DMS oxidation. Possible explanations include the difference in DMS emission rates, which are higher in our model at high latitudes where DMS oxida-

tion is slower. The lifetime of DMS in the GISS model is very close to that in our model, although the DMS burden is lower in the GISS model, probably due to the lower emission rates.

The lifetime of 2.6 days for SO<sub>2</sub> in the GISS model is about 40% longer than the ones in both our model (1.8 days) and the NCAR model (1.9 days), reflecting a slower removal rate in the GISS model. Regarding the lifetime of sulfate, we estimate a value of 5.8 days with respect to the sulfate dry deposition and wet scavenging. If we had included the amount of SO<sub>2</sub> lost by wet scavenging as a sink of sulfate, as the GISS and NCAR models have, then the sulfate lifetime in our model would be 4.6 days, which is lower than the GISS model but higher than the NCAR model. The point we try to make here is that the atmospheric sulfate residence time is underestimated when wet scavenging of SO<sub>2</sub> is included as a loss term of sulfate. The lifetime of DMS is similar to that in the GISS model but higher than that in the NCAR model, whereas the lifetime of MSA is slightly lower than that in the GISS model (MSA is not simulated in the NCAR model).

To examine the differences between the models in loss rates for individual sinks, we list in Table 2 the loss frequencies for each process, defined as the SO<sub>2</sub> or sulfate atmospheric burden divided by their individual removal rates. While dry removal processes for SO<sub>2</sub> (dry deposition and in-air oxidation) are the most efficient in our model, wet processes (aqueous phase production and wet removal) are the most effective in the NCAR model but the least effective in the GISS model. The effectiveness of the wet process is almost inversely proportional to the SO<sub>2</sub> and sulfate burden, which are the lowest in the NCAR model and highest in the GISS model. For example, a ratio of the sulfate burden between the GOCART, GISS, and NCAR models is 1:1.3:0.9, and that of the SO<sub>2</sub> burden is 1:1.2:0.9, which is also the ratio of the inverse of the total sulfur wet deposition rate. Interestingly, the sulfate burden is also inversely proportional to the wet production rate of sulfate (in-cloud and in-rain); a ratio of 1:1.1:0.9 is found between the three models. These linear relations clearly confirm the importance of the wet processes in determining the sulfur burden in the atmosphere. Therefore emphasis should be given to improving the wet physical and chemical processes and validating the parameters used in modeling these processes, such as cloud distribution, cloud fractions, precipitation amount, scavenging efficiencies, and the aqueous phase oxidation rates.

Comparing our zonally averaged concentrations of SO<sub>2</sub>, sulfate, and DMS in Figure 5 with those reported by Koch *et al.* [1999] and Barth *et al.* [2000], we find that the SO<sub>2</sub> concentrations in the GISS model are significantly higher than those in both the NCAR and our model in the lower troposphere. For example, a 500 ppt SO<sub>2</sub> contour in the GISS model reached 700 mbar and extended from 27°N to 75°N, while this contour line is confined below 850 mbar and at the latitudes

between 25°N and 60°N in both the NCAR and our models. A similar difference in sulfate distribution is also found. Our extratropical DMS zonal distribution resembles that in the GISS model with a symmetric distribution between the northern and southern hemispheres. However, in the tropical upper troposphere, there is a second maximum of DMS in our model with a concentration of 5–10 ppt, a feature which is very similar to the NCAR model but not obvious in the GISS model.

The results from the GOCART model differ from those of Chin *et al.* [1996] (using the Harvard/GISS GCM II model) in a number of ways. The major difference is in the sulfate vertical distributions. The zonally averaged sulfate distribution in Figure 5 shows a much less vertical gradient than that of Chin *et al.* [1996]. The difference is attributed mainly to a much more efficient wet scavenging in the work of Chin *et al.* [1996], partly due to the excessive wet convection over some regions, and partly due to the higher wet scavenging efficiency (100% in deep wet convection). The other difference is in DMS oxidation. Chin *et al.* [1996] found that an oxidant in addition to OH and NO<sub>3</sub> was needed for DMS oxidation in order to reproduce both DMS and sulfate concentrations observed over the remote ocean surface. We do not invoke such an oxidant in this study, and our simulated concentrations for all sulfur species are overall consistent with the observations over the oceans [Chin *et al.*, this issue]. We attribute this difference to the better parameters in calculating the DMS emission rates and the higher (a factor of 2 to 3) OH concentrations over the ocean surface (a factor of 2 to 3) used in this study than those used by Chin *et al.* [1996].

## 5. Anthropogenic Contributions

We have conducted a model simulation for 1990 without anthropogenic emissions in order to estimate the relative importance of natural and anthropogenic sources to the atmospheric sulfate loading. The total emission for this case is 18.8 Tg S yr<sup>-1</sup>, which includes only the DMS and volcanic SO<sub>2</sub> sources. The annually averaged column sulfate burden and the anthropogenic contributions for 1990 are shown in Figure 7. The anthropogenic fraction of sulfate is more than 60% in the northern hemisphere, with more than 80% over the United States and the Eurasian continent. A more widely spread anthropogenic influence over the northern hemisphere is found in the GISS [Koch *et al.*, 1999] and NCAR [Rasch *et al.*, 2000] models, with more than 80% anthropogenic sulfate over the entire area at latitudes north of 10°N. In the southern hemisphere the anthropogenic fraction is generally 20–40% over the ocean in our model (Figure 8), similar to the GISS and NCAR models.

We find that anthropogenic sources contribute to 67% of the total sulfate burden in 1990, a fraction which is somewhat lower than the anthropogenic sulfur emission



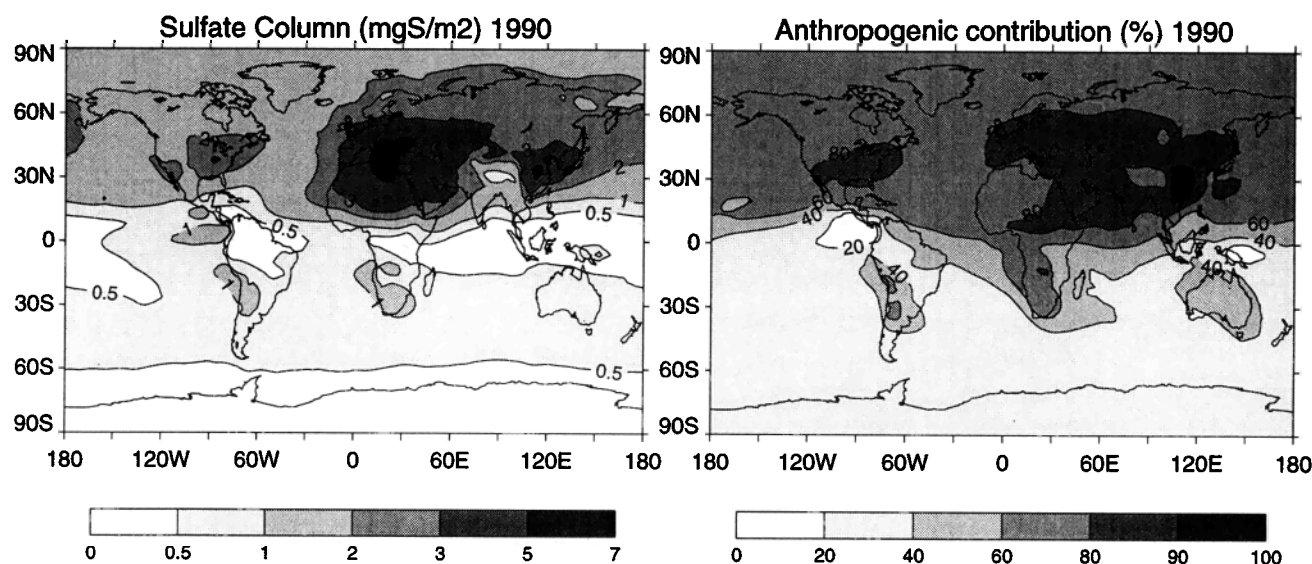


**Figure 7.** Total sulfate column burden ( $\text{mg S m}^{-2}$ ) and the anthropogenic fraction in the 1990 simulation.

fraction of 80%. Figure 8 shows the percentage of zonally averaged anthropogenic contribution for two seasons, DJF and JJA, in 1990. As can be seen in Figure 8, the anthropogenic sulfate dominates the sulfate burdens in the northern hemisphere but with distinct patterns between DJF and JJA. It disperses horizontally in DJF with the 80% contourline stretched out to the northern polar region but confined below 600 mbar. By contrast, the anthropogenic sulfate is well mixed vertically by the frequent convective activities in JJA with the 80% contour line extended to the tropopause. Of interest is that the anthropogenic contribution increases with the altitude over the mid to high latitude in the southern hemisphere, resulting from the interhemispheric transport from the northern hemisphere and the convective transport from the midlatitudes.

When comparing the natural sulfur budget with that in the GISS model [Koch *et al.*, 1999], a major disagreement lies in the lifetimes of  $\text{SO}_2$  and sulfate. While in

the GISS model the  $\text{SO}_2$  lifetime from a natural-source-only run (1.8 days) was shorter than that from a full run (2.6 days), we find that the reverse is the case in our model: 2.4 days in the natural-source-only run and 1.8 days in the full run. As for sulfate, the lifetime stayed the same in both natural and full simulations in the GISS model, but in our model it is longer from the natural simulation (7.2 days) than that from the full simulation (5.8 days). It is expected that  $\text{SO}_2$  and sulfate of natural origin should have a longer lifetime than the anthropogenic ones because they are not as concentrated near the surface, thus not subject to the fast removal by dry and wet depositions.

The anthropogenic contribution to the atmospheric sulfate burden from this study, as well as from the GISS and NCAR models, is significantly higher than that reported by Chin and Jacob [1996]. The latter study found that the anthropogenic sources contributed to only 37% of the sulfate burden, although they ac-

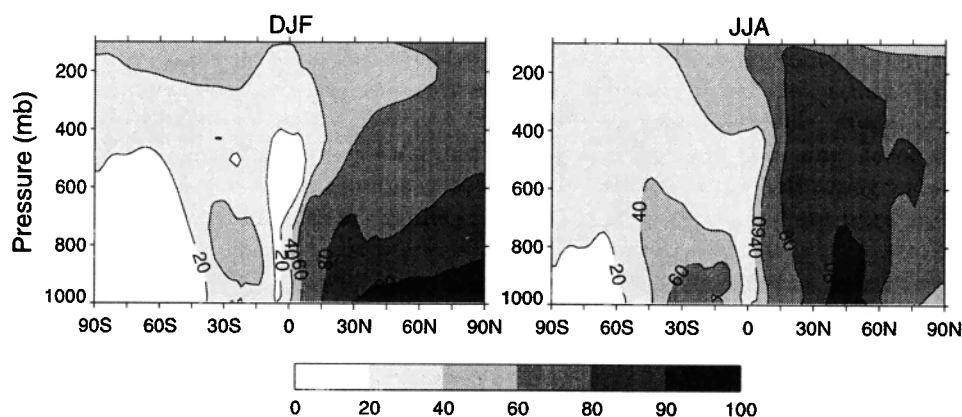


**Figure 8.** Zonally averaged anthropogenic sulfate fraction in DJF and JJA in the 1990 simulation.

counted for 70% of the total sulfur emission. This is due to the high sulfate production rates from DMS oxidation and more excessive wet scavenging near the mid-latitude continents in the work of *Chin et al.* [1996] than those in this study.

## 6. Conclusions

We have used the GOCART model to simulate the tropospheric sulfur cycle. The model uses the assimilated meteorological fields from the GEOS DAS, making it potentially the best tool to link the satellite and in situ observations for global analysis. We have incorporated in the model the most updated emission inventories of anthropogenic, biogenic, and volcanic sources for DMS and SO<sub>2</sub>. In a typical year without major volcanic eruptions, we estimate that about 20% of the sulfate precursor emission is from natural sources (biogenic and volcanic) while 80% is anthropogenic. In-air and in-cloud oxidation of SO<sub>2</sub> account for 36% and 64%, respectively, of the atmospheric sulfate production. We have estimated a sulfate production efficiency as a ratio of the amount of sulfate produced to the total amount of SO<sub>2</sub> emitted and produced in the atmosphere. A typical production efficiency value of 0.41–0.42 is found, indicating that generally more than half of the SO<sub>2</sub> entering the atmosphere does not contribute to the sulfate production but is either removed by dry deposition or scavenged by the rain. We have reported that in 1990 the atmospheric burdens for SO<sub>2</sub>, sulfate, DMS, and MSA are 0.43, 0.63, 0.073, and 0.028 Tg S, respectively, with the corresponding lifetimes of 1.8, 5.8, 2.0, and 7.1 days.

The anthropogenic contribution to the atmospheric sulfate burden is estimated at 67% for 1990, a fraction which is somewhat smaller than that of anthropogenic emission (80%). While it is horizontally spreading out to the northern polar region in DJF, the anthropogenic contribution is vertically well mixed in JJA, with the 80% contour line extended to the tropopause over the midlatitudes in the northern hemisphere. We have also shown that major volcanic eruptions can significantly change the sulfate formation pathways, distributions, abundance, and lifetime. These effects are seen in our model simulations from 1989 to 1994, a period which includes the major volcanic eruption of Mount Pinatubo in 1991. It has been demonstrated that while SO<sub>2</sub> returns to its normal level in only a few months after the Pinatubo eruption, it takes several years for sulfate to relax back to its normal atmospheric loading.

Our model results of 1990 have been compared with two most recent model studies, namely, the GISS model [*Koch et al.*, 1999] and the NCAR model [*Barth et al.*, 2000; *Rasch et al.*, 2000]. While the annual DMS burden in our model is 20–30% larger than the other two models, our SO<sub>2</sub> and sulfate burdens are lower than those in the GISS model but higher than those in the NCAR model. The relative abundance of the SO<sub>2</sub> and

sulfate burden is almost inversely proportional to the rate of wet removal and the rate of wet production of sulfate. This proportionality shows the magnitude of the wet processes in controlling the atmospheric sulfur burden. Therefore the first priority in future research should be to reduce the large uncertainties associated with the wet physical and chemical processes.

**Acknowledgments.** We thank Daniel Jacob of Harvard University for many helpful discussions and his comments on this manuscript. We thank Andrea Molod of GSFC for helping with the GEOS data, Joe Ardizzone of GSFC for providing the SSM/I winds, Paul Houser of GSFC for providing the merged precipitation products, Paul Ginoux of Georgia Tech/GSFC for obtaining the GEOS turbulent coefficients, Lee Siebert and Tom Simkin of Smithsonian Institution Global Volcanism Program for providing chronological volcanic eruption data, Lori Glaze and Arlin Krueger of GSFC for discussions of volcanic emissions, Ulrike Lohmann of Dalhousie University for providing cloud fraction formula, and the EDGAR database for providing 1990 SO<sub>2</sub> emission inventory. Comments from two anonymous reviewers are gratefully acknowledged. This research is sponsored by the NASA Atmospheric Chemistry Modeling and Analysis Program, Global Aerosol Climatology Program, EOS/Interdisciplinary Science Program, Goddard Space Flight Center, and NOAA Aerosol Program.

## References

- Allen, D. J., P. Kasibhatla, A. M. Thompson, R. B. Rood, B. G. Doddridge, K. E. Pickering, R. D. Hudson, and S.-J. Lin, Transport-induced interannual variability of carbon monoxide determined using a chemistry and transport model, *J. Geophys. Res.*, **101**, 28,655–28,669, 1996.
- Andres, R. J., and A. D. Kasgnoc, A time-averaged inventory of subaerial volcanic sulfur emissions, *J. Geophys. Res.*, **103**, 25,251–25,261, 1998.
- Atlas, R., R. N. Hoffman, S. C. Bloom, J. C. Jusem, and J. Ardizzone, A multiyear global surface wind velocity dataset using SSM/I wind observations, *Bull. Am. Meteorol. Soc.*, **77**, 869–882, 1996.
- Balkanski, Y. J., D. J. Jacob, G. M. Gardner, W. C. Graustein, and K. K. Turekian, Transport and residence times of tropospheric aerosols inferred from a global three-dimensional simulation of <sup>210</sup>Pb, *J. Geophys. Res.*, **98**, 20,573–20,586, 1993.
- Barth, M., P. J. Rasch, J. T. Kiehl, C. M. Benkovitz, and S. E. Schwartz, Sulfur chemistry in the National Center for Atmospheric Research Community Climate Model: Description, evaluation, features and sensitivity to aqueous chemistry, *J. Geophys. Res.*, **105**, 1387–1415, 2000.
- Bates, T. S., B. K. Lamb, A. Guenther, J. Dignon, and R. E. Stoiber, Sulfur emissions from natural sources, *J. Atmos. Chem.*, **14**, 315–337, 1992.
- Benkovitz, C. M., M. T. Scholtz, J. Pacyna, L. Tarrason, J. Dignon, E. C. Voldner, P. A. Spiro, J. A. Logan, and T. E. Graedel, Global gridded inventories of anthropogenic emissions of sulfur and nitrogen, *J. Geophys. Res.*, **101**, 29,239–29,253, 1996.
- Berresheim, H., J. W. Huey, R. P. Thorn, F. L. Eisele, D. J. Tanner, and A. Jefferson, Measurements of dimethyl sulfide, dimethyl sulfoxide, dimethyl sulfone, and aerosol ions at Palmer Station, Antarctica, *J. Geophys. Res.*, **103**, 1629–1637, 1998.
- Bluth, G. J. S., W. I. Rose, I. E. Sprod, and A. J. Krueger, Stratospheric loading of sulfur from explosive volcanic eruptions, *J. Geol.*, **105**, 671–683, 1997.



- Chin, M., and D. J. Jacob, Anthropogenic and natural contributions to tropospheric sulfate: A global model analysis, *J. Geophys. Res.*, **101**, 18,691-18,699, 1996.
- Chin, M., D. J. Jacob, G. M. Gardner, M. S. Foreman-Fowler, and P. A. Spiro, A global three-dimensional model of tropospheric sulfate, *J. Geophys. Res.*, **101**, 18,667-18,690, 1996.
- Chin, M., R. B. Rood, D. J. Allen, M. O. Andreae, A. M. Thompson, S.-J. Lin, R. M. Atlas, and J. V. Ardizzone, Processes controlling dimethyl sulfide over the ocean: Case studies using a 3-D model driven by assimilated meteorological fields, *J. Geophys. Res.*, **103**, 8341-8353, 1998.
- Chin, M., D. L. Savoie, B. J. Huebert, A. R. Bandy, D. C. Thornton, T. S. Bates, P. K. Quinn, E. S. Saltzman, and W. J. De Bruyn, Atmospheric sulfur cycle simulated in the global model GOCART: Comparison with field observations and regional budgets, *J. Geophys. Res.*, this issue.
- Chuang, C. C., J. E. Penner, K. E. Taylor, A. S. Grossman, and J. J. Walton, An assessment of the radiative effects of anthropogenic sulfate, *J. Geophys. Res.*, **102**, 3761-3778, 1997.
- Cohan, D. S., M. G. Schultz, D. J. Jacob, B. G. Heikes, and D. R. Blake, Convective injection and photochemical decay of peroxides in the tropical upper troposphere: Methyl iodide as a tracer of marine convection, *J. Geophys. Res.*, **104**, 5717-5724, 1999.
- Dana, M. T., and J. M. Hales, Statistical aspects of the washout of polydisperse aerosols, *Atmos. Environ.*, **10**, 45-50, 1976.
- Daum, P. H., S. E. Schwartz, and L. Newman, Acidic and related constituents in liquid-water clouds, *J. Geophys. Res.*, **89**, 1447-1458, 1984.
- DeMore, W. B., S. P. Sander, D. M. Golden, R. F. Hampson, M. J. Kurylo, C. J. Howard, A. R. Ravishankara, C. E. Kolb, and M. J. Molina, Chemical kinetics and photochemical data for use in stratospheric modeling, Evaluation number 12, *JPL Publ.* 97-4, 1997.
- Erickson, D. J., III, A stability-dependent theory for air-sea gas exchange, *J. Geophys. Res.*, **98**, 8471-8488, 1993.
- Feichter, J., E. Kjellstrom, H. Rodhe, F. Dentener, J. Lelieveld, and G.-J. Roelofs, Simulation of the tropospheric sulfur cycle in a global climate model, *Atmos. Environ.*, **30**, 1693-1708, 1996.
- Ganzeveld, L., J. Lelieveld, and G.-J. Roelofs, A dry deposition parameterization for sulfur oxides in a chemistry and general circulation model, *J. Geophys. Res.*, **103**, 5679-5694, 1998.
- Giorgi, F., and W. L. Chameides, Rainout lifetimes of highly soluble aerosols and gases as inferred from simulations with a general circulation model, *J. Geophys. Res.*, **91**, 14,367-14,376, 1986.
- Helfand, H. M., and J. C. Labraga, Design of a nonsingular level 2.5 second-order closure model for the prediction of atmospheric turbulence, *J. Atmos. Sci.*, **45**, 113-132, 1988.
- Huffman, G. J., et al., The Global Precipitation Climatology Project (GPCP) combined precipitation data set, *Bull. Am. Meteorol. Soc.*, **78**, 5-20, 1997.
- Kettle, A. J., et al., A global database of sea surface dimethylsulfide (DMS) measurements and a simple model to predict sea surface DMS as a function of latitude, longitude, and month, *Global Biogeochem. Cycles*, **13**, 399-444, 1999.
- Koch, D., D. Jacob, I. Tegen, D. Rind, and M. Chin, Tropospheric sulfur simulation and sulfate direct radiative forcing in the GISS GCM, *J. Geophys. Res.*, **104**, 23,799-23,823, 1999.
- Langner, J., and H. Rodhe, A global three-dimensional model of the tropospheric sulfur cycle, *J. Atmos. Chem.*, **13**, 225-263, 1991.
- Lin, S.-J., and R. B. Rood, Multidimensional flux-form semi-Lagrangian transport schemes, *Mon. Weather Rev.*, **124**, 2046-2070, 1996.
- Liss, P. S., and L. Merlivat, Air-sea gas exchange rates: Introduction and synthesis, in *The Role of Air-Sea Exchange in Geochemical Cycling*, edited by P. Buat-Ménard, D. Riedel, pp. 113-127, Norwell, Mass., 1986.
- McCormick, M. P., L. W. Thomason, and C. R. Trepte, Atmospheric effects of the Mt. Pinatubo eruption, *Nature*, **373**, 309-404, 1995.
- Müller, J.-F., and G. Brasseur, IMAGES: A three-dimensional chemical transport model of the global troposphere, *J. Geophys. Res.*, **100**, 16,445-16,490, 1995.
- Olivier, J. G. J., A. F. Bouwman, C. W. M. Van der Maas, J. J. M. Berdowski, C. Veldt, J. P. J. Bloss, A. J. H. Vesschedijk, P. Y. J. Zandveld, and J. L. Haverlag, Description of EDGAR Version 2.0: A set of global emission inventories of greenhouse gases and ozone-depleting substances for all anthropogenic and most natural sources on a per country basis and on  $1^\circ \times 1^\circ$  grid, *RIVM/TNO Rep. 771060 002*, Rijkinstituut voor Volksgezondheid en Milieu, Bilthoven, Netherlands, Dec. 1996.
- Pham, M., J.-F. Müller, G. Brasseur, C. Granier, and G. Megie, A three-dimensional study of the tropospheric sulfur cycle, *J. Geophys. Res.*, **100**, 26,061-26,092, 1995.
- Rasch, P. J., M. C. Barth, J. T. Kiehl, S. E. Schwartz, and C. M. Benkovitz, A description of the global sulfur cycle and its controlling processes in the National Center for Atmospheric Research Community Climate Model, Version 3, *J. Geophys. Res.*, **105**, 1367-1385, 2000.
- Roelofs, G.-J., J. Lelieveld, and L. Ganzeveld, Simulation of global sulfate distribution and the influence on effective cloud drop radii with a coupled photochemistry-sulfur cycle model, *Tellus, Ser. B*, 224-242, 1998.
- Saltzman, E. S., D. B. King, K. Holmen, and C. Leck, Experimental determination of the diffusion coefficient of dimethylsulfide in seawater, *J. Geophys. Res.*, **98**, 16,481-16,486, 1993.
- Sandnes, H., and H. Styve, Calculated budgets for airborne acidifying components in Europe, 1985, 1987, 1988, 1989, 1990 and 1991, *EMEP/MS-CW Rep. 1/92*, Norw. Meteorol. Inst., Oslo, Norway, 1992.
- Schnetzler, C. C., G. J. S. Bluth, A. J. Krueger, and L. S. Walter, A proposed volcanic sulfur dioxide index (VSI), *J. Geophys. Res.*, **102**, 20,087-20,091, 1997.
- Schubert, S. D., R. B. Rood, and J. Pfendner, An assimilated data set for earth science applications, *Bull. Am. Meteorol. Soc.*, **74**, 2331-2342, 1993.
- Smethie, W. M., Jr., T. Takahashi, D. W. Chipman, and J. R. Ledwell, Gas exchange and  $\text{CO}_2$  flux in the tropical Atlantic Ocean determined from  $^{222}\text{Rn}$  and  $\text{pCO}_2$  measurements, *J. Geophys. Res.*, **90**, 7005-7022, 1985.
- Simkin, T., and L. Siebert, *Volcanoes of the World*, 2nd ed., Geosci., Tucson, Ariz., 1994.
- Spiro, P. A., D. J. Jacob, and J. A. Logan, Global inventory of sulfur emissions with  $1^\circ \times 1^\circ$  resolution, *J. Geophys. Res.*, **97**, 6023-6036, 1992.
- Staubs, R., and H.-W. Georgii, Biogenic sulfur compounds in seawater and the atmosphere of the Antarctic region, *Tellus, Ser. B*, 127-137, 1993.
- Sundqvist, H., E. Berge, and J. E. Kristiansson, Condensation and cloud parameterization studies with a mesoscale numerical weather prediction model, *Mon. Weather Rev.*, **117**, 1641-1657, 1989.
- Suzuki, T., A theoretical model for dispersion of tephra, in *Arc Volcanism: Physics and Tectonics*, edited by D.

- Shimozuru and I. Yokoyama, pp. 95-113, Terra Sci. Pub., Tokyo, 1983.
- Takacs, L. L., A. Molod, and T. Wang, Documentation of the Goddard Earth Observing System (GEOS) general circulation model - version 1, *NASA Tech. Memo., TM-104606, vol. 1*, 1994.
- Tarrason, L., and T. Iversen, Modeling intercontinental transport of atmospheric sulphur in the northern hemisphere, *Tellus, Ser. B*, 331-352, 1998.
- Voldner, E. C., L. A. Barrie, and A. Sirois, A literature review of dry deposition of oxides of sulphur and nitrogen with emphasis on long-range transport modelling in North America, *Atmos. Environ.*, 20, 2101-2123, 1986.
- Walcek, C. J., R. A. Brost, J. S. Chang, and M. L. Wesely, SO<sub>2</sub>, sulfate and HNO<sub>3</sub> deposition velocities computed using regional land use and meteorological data, *Atmos. Environ.*, 20, 949-964, 1986.
- Wanninkhof, R., Relationship between wind speed and gas exchange over the ocean, *J. Geophys. Res.*, 97, 10,757-10,768, 1992.
- Weisenstein, D. K., M. K. W. Ko, N.-D. Sze, and J. M. Rodriguez, Potential impact of SO<sub>2</sub> emissions from stratospheric aircraft on ozone, *Geophys. Res. Lett.*, 23, 161-164, 1996.
- Wesely, M. L., Parameterization of surface resistance to gaseous dry deposition in regional-scale numerical models, *Atmos. Environ.*, 23, 1293-1304, 1989.
- Wesely, M. L., and B. B. Hicks, Some factors that affect the deposition rates of sulfur dioxide and similar gases on vegetation, *J. Air Pollut. Control Assoc.*, 27, 1110-1116, 1977.
- Xu, K.-M., and S. K. Krueger, Evaluation of cloudiness parameterizations using a cumulus ensemble model, *Mon. Weather Rev.*, 119, 342-367, 1991.

---

M. Chin (corresponding author), S.-J. Lin, R. B. Rood, and A. M. Thompson, Laboratory for Atmospheres, NASA Goddard Space Flight Center, Greenbelt, MD 20771. (chin@rondo.gsfc.nasa.gov; slin@dao.gsfc.nasa.gov; rood@dao.gsfc.nasa.gov; thompson@gator1.gsfc.nasa.gov)

J.-F. Müller, Belgian Institute for Space Aeronomy, Brussels, Belgium. (Jean-Francois.Muller@bira-iasb.oma.be)

(Received March 23, 2000; revised June 15, 2000; accepted June 16, 2000.)